# Superradiance in a Torus Magnetosphere Around a Black Hole

Maurice H. P. M. van Putten

The coalescence of a neutron star and a black hole in a binary system is believed to form a torus around a Kerr black hole. A similarly shaped magnetosphere then results from the remnant magnetic field of the neutron star. In the strong-field case, it contains a cavity for plasma waves located between the barrier of the gravitational potential and the surrounding torus. This cavity may be unstable to superradiance of electromagnetic waves. Superradiant amplification of such waves, initially excited by turbulence in the torus, should inflate into a bubble in a time as short as $\sim$0.75 (1 percent/$|\epsilon|^2$)($M/7M_\odot$) seconds $\sim$0.15 to 1.5 seconds, assuming an efficiency $|\epsilon|^2 = 0.5$ to 5 percent and a mass $M = 7M_\odot$. These bubbles may burst and repeat, of possible relevance to intermittency in cosmological $\gamma$-ray bursts. The model predicts $\gamma$-ray bursts to be anticorrelated with their gravitational wave emissions.

Binary systems of stars and their formation play a central role in continuous and transient high-energy phenomena. Accreting binaries, for example, are bright x-ray sources with persistent and highly time-variable behavior around neutron stars or black-hole candidates (*1*). Given the observed neutron-star/neutron-star binaries (*2*), it is believed that neutron-star/black-hole (NS/BH) binaries exist as well. These systems may be observed only if the neutron star is a pulsar or when the neutron star is disrupted by the black hole. The coalescence of a NS/BH binary has been proposed as a model for cosmological $\gamma$-ray bursts (*3*, *4*). Although the masses of black-hole candidates may well be similar (*5*), their angular momenta and hence their spin energies are not expected to show a narrow distribution. This likely variety in energy available from the black-hole partners seems consistent with the diversity in the observed $\gamma$-ray bursts (*3*).

The evolution of a NS/BH system is driven primarily by the emission of gravitational radiation. As the system approaches coalescence, the neutron star becomes susceptible to tidal breakup if the black-hole mass $M$ is on the order of a few solar masses $M_\odot$. The equation of state of the neutron star matter and the process of breakup remain uncertain. Early circularization of the neutron star orbit favors the formation of a torus, while heating and phase transitions may disrupt the flow of the debris. Lattimer and Schramm (*6*) argued that mass loss from the neutron star during breakup is less than 5%. If the breakup takes place outside the innermost stable circular orbit (ISCO) of the black hole, the debris is expected to form a torus, while inside the ISCO the debris will accrete directly onto the black hole. The orbital separation during breakup is determined by the mean mass density $\rho_{NS}$ of the neutron star, the black hole mass $M$, and its specific angular momentum $a$. Breakup of the neutron star takes place outside the ISCO if $\rho_{NS}$ is sufficiently low; typically $\rho_{NS} < 1.4 \times 10^{16}(M_\odot/M)^2$ g cm$^{-3}$ around a nonrotating or Schwarzschild black hole (*7*), and $\rho_{NS} < 7.8 \times 10^{17}$ $(M_\odot/M)^2$ g cm$^{-3}$ around a maximally spinning Kerr black hole (*8*), both for mildly relativistic orbits (*9*). For a canonical value $\rho_{NS} = 10^{15}$ g cm$^{-3}$, and therefore breakup is expected to take place outside the ISCO of a Schwarzschild black hole when $M \leq 3.7M_\odot$, and outside the ISCO of an extreme Kerr black hole when $M \leq 28M_\odot$. By this estimate a torus is most likely to form around a Kerr black hole that spins rapidly (*3*). Fortunately, stellar-mass black holes are believed to result from core collapse (*10*), and this almost certainly produces black holes with high rotation (*11*). Once a torus has formed outside the ISCO, it is expected to evolve on a secular time scale before further breakup. Not much is known about the instabilities of a strongly self-gravitating torus. These tori may be susceptible to secular instabilities such as those in rapidly spinning neutron stars [see, for example, (*12*) for the Chandrasekhar-Friedman-Schutz instability], but on the time scales of $\gamma$-ray bursts such effects are probably unimportant.

The torus is presumably magnetized with the remnant magnetic field from the former neutron star. To leading order, I estimate its large-scale magnetic field $B$ to be as shown in Fig. 1. The black hole and the magnetic field interact in a manner that could be described as either open or closed, depending on whether the field lines penetrating the black hole connect, respectively, to infinity or to a surrounding accretion disk or torus. A black hole that rotates at an angular velocity $\Omega_H$ interacts with its magnetosphere like $\Omega_H \dot{J}_H + D_H + L_H = 0$, where $-\Omega_H \dot{J}_H$ is the work done by the angular momentum $J_H$ of the black hole, $D_H$ is the dissipation in the horizon, and $L_H$ is its luminosity. From the first law of black-hole thermodynamics (*13*), it follows that $L_H = -\dot{M}$, where $\dot{M}$ is the rate of change of mass-energy of the black hole as measured at infinity. In the closed model at hand, $L_H$ is deposited into the torus. This torus is subject to a spin-up torque $T = -\dot{J}_H$ and to a spin-down torque resulting from emission of radio waves to infinity, similar to that in pulsars (*14*). If the latter torque is small, there exists a critical value $R_c \sim 2\sqrt{3}\, M^{3/2} m_T^{-1/2}$ for the major radius $R$ of a torus with mass $m_T$, within (outside) which a black-hole/torus equilibrium state is unstable (stable) against angular momentum transfer by way of the inner magnetosphere.

The magnetic field near the horizon is approximately the superposition of two Wald fields, but perturbed by a twist resulting from poloidal currents. A Wald field (*15*) is radial on the horizon and vanishes at the equator (*16*). The torus magnetosphere rotates with the Keplerian angular velocity $\omega_T = M^{1/2}/(R^{3/2} + aM^{1/2}) \sim M^{1/2}R^{-3/2}$ of the torus (*17*). Corotation extends from the inner (ils) to the outer (ols) light surfaces (*18*, *19*). The ils and ols are limiting surfaces, beyond which the angular velocity of particles leads (inside the ils) or lags (outside the ols) to avoid superluminal motion. Generally, particles flow outward along azimuthally bent field lines

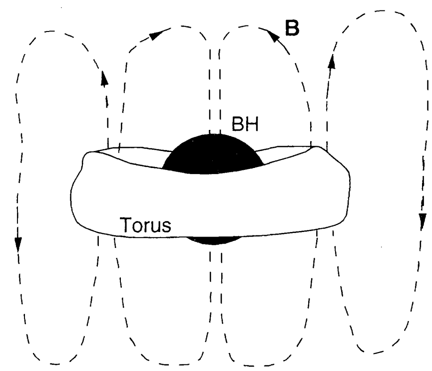


**Fig. 1.** Cartoon of a torus magnetosphere around a black hole. The torus may form from the breakup of a neutron star around a rapidly spinning Kerr black hole of a few solar masses (*3*, *9*). The magnetosphere is a remnant of the field from the neutron star. Shown is a "bipolar" magnetic field, produced by two concentric current loops with opposite orientations. These loops result topologically from winding a single loop once around the black hole followed by a reconnection. The inner part of the magnetosphere couples the torus to the black hole. The outer part couples the torus to infinity in a process similar to that in pulsars. An instability is described for the inner part.

Massachusetts Institute of Technology, Cambridge, MA 02139, USA. E-mail: mvp@math.mit.edu

beyond the ols and flow inward within the ils toward the horizon. These surfaces are given by the null condition $0 = g_{tt} + 2g_{\phi t}\omega_T + g_{\phi\phi}\omega_T^2$ in terms of the metric $g_{\alpha\beta}$ (*19*). The ils touches the last closed field line in corotation with the torus, whereas the open field lines inside the ils connect the torus with the horizon (Fig. 2). The last closed field line encloses a trapped region that I term a "bag." By symmetry, the field vanishes in an equatorial annulus between the horizon and the ils. This annulus, where $B = 0$, is a defect in the magnetosphere with important implications.

The Blandford-Znajek process (*19*) induces a poloidal current loop in the magnetosphere by virtual polarization of the horizon. This loop consists of magnetic field–lines, the torus and its bag, and spark gaps in the polar currents $I$ and in the equatorial current $I_S$. A Poynting flux $S$ is produced. It generally extracts energy from the black hole when the latter spins faster than the torus. In force-free condition, the scalar $\phi = F_{ab}F^{ab}$ of the electromagnetic field tensor $F_{ab}$ produces poloidal surfaces $\phi$ = constant that contain both the magnetic field–lines and the current density $j^b$. If the poloidal component of $j^b$ vanishes somewhere, then it vanishes everywhere on a given surface $\phi$ = constant. The $B = 0$ annulus contains an electric field $E \sim B(1 - \omega_T/\Omega_H)a/d$, assuming a gap width $d$. Although $E$ is large, it need not satisfy $E > B$ at the tip of the bag to tap its charged particles in establishing $I_S$. It may produce $I_S$ by vacuum breakdown, however—for example, by the Schwinger process. By dissipation, the annulus produces and absorbs a poloidal Poynting flux. This strips neighboring surfaces $\phi$ = constant of their charged particles and leaves them almost completely depleted near the horizon. No net current is associated with this process; hence, these surfaces are free of poloidal current everywhere. Combined, they trace out a cavity from the horizon to the torus that is essentially free of poloidal current. The return current $I$ proceeds at higher latitudes. This yields $L_H \sim \omega_T(\Omega_H - \omega_T)(a/M)^2B^2M^2/32\Omega_H^2$, as shown in Thorne *et al.* (*13*).

In the Blandford-Znajek process, electron-positron pairs are produced in the current-carrying section of the magnetosphere. These pairs establish a force-free plasma when $B$ exceeds the critical value $B_c = 20(M/a)^{3/4}(M_\odot/M)^{1/2}10^4$ G. Flux conservation and magnetic field–winding imply $B$ to be larger than its progenitor value $B \sim 10^{15}$ to $10^{17}$ G. Because $B$ exceeds $B_c$ by about 10 orders of magnitude, the current-carrying section of the magnetosphere is expected to be a hot and dense plasma and to be saturated with γ-rays from pair production. Although more detailed calculations would be desirable, this qualitative picture already describes a state of ideal magnetohydrodynamics, possibly also force-free, that encloses the cavity.

Two plasma waves exist in the cavity—the fast magnetosonic waves and the Alfvén waves (*20*, *21*). The fast magnetosonic waves are linearly polarized electromagnetic waves in the force-free limit. Both propagate in a curved space-time background. This background contains an inner barrier produced by the rotation of the black hole. Waves of positive energy can be excited by the torus when it extends beyond this barrier. The torus may consist of matter resembling that in neutron stars (*7*, *22*). However, a dimensional analysis indicates a steep drop in density of up to five orders of magnitude below $\rho_{NS}$, implying that the torus is more likely to be in a state of high-density white-dwarf matter. The electrical conductivity of such matter is large (*23*), indicating a high reflectivity of the surface of the torus. Because of the ideal magnetohydrodynamics in the surrounding plasma, the cavity thus becomes a waveguide not only for Alfvén waves, but also for the fast magnetosonic waves. In many ways, this cavity resembles the vacuum cavity around a black hole enclosed by a spherical mirror (*24*).

The rotation of the black hole interacts with bosonic fields by superradiance (*24*–*26*) for waves of frequency $0 < \omega < m\Omega_H$ and of azimuthal quantum number $m$. It is the long-wavelength analog of the Penrose process (*17*), whereby an incoming wave with positive energy splits up into a transmitted wave with negative energy and a reflected wave with enhanced positive energy. The negative-energy wave propagates into the black hole, equivalent to a positive-energy wave coming out of the horizon (*26*, *27*). For a force-free plasma, it has been shown explicitly in the WKB approximation that the magnetosonic wave scatters superradiantly, although the Alfvén wave does not (*21*).

Superradiance of scalar (spin 0), electromagnetic (spin 1), or gravitational (spin 2) waves is qualitatively similar to each other and increases with higher spin (*28*). Although desirable, calculation of superradiance of the fast magnetosonic waves falls outside the scope of this work. However, a worst-case estimate can be obtained from a massless scalar field $\Phi$. I calculated $\Phi$ in a cavity formed by a toroidal wedge with constant opening angle. In Boyer-Linquist coordinates, $\Phi$ satisfies

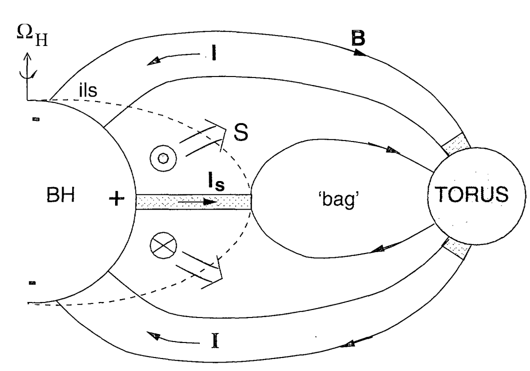


**Fig. 2.** A schematic cross section of the torus magnetosphere. The magnetosphere rotates with the Keplerian angular velocity of the torus. Corotation extends down to the inner light surface (ils) (*18*, *19*). The ils touches the last closed field line from the torus, which encloses a trapped region nicknamed the "bag." The black hole and the torus are coupled by the open field lines $B$ that close on the horizon. The Blandford-Znajek process (*19*) generates a poloidal current loop by virtual polarization of the horizon. A current $I$ flows along open field lines, the torus, and the bag, through a spark with net current $I_S = 2I$ and closes over the horizon. A Poynting flux $S$ emerges from the horizon that extracts energy from the black hole, if it spins more rapidly than the torus. The outer layers carry a current $I$ by virtue of spark gaps on the surface of the torus and are in a state of ideal magnetohydrodynamics. Near the horizon, the poloidal magnetic field is similar to a Wald field (*15*), but with a toroidal field component resulting from the poloidal currents. The spark current $I_S$ flows in a $B = 0$ annulus and is due to vacuum breakdown. The associated dissipation depletes neighboring open field lines from particles, whereby they become essentially current free. Combined, these field lines trace out a current-free cavity in the magnetosphere. The cavity, enclosed by ideal magnetohydrodynamics, becomes a waveguide for plasma waves.

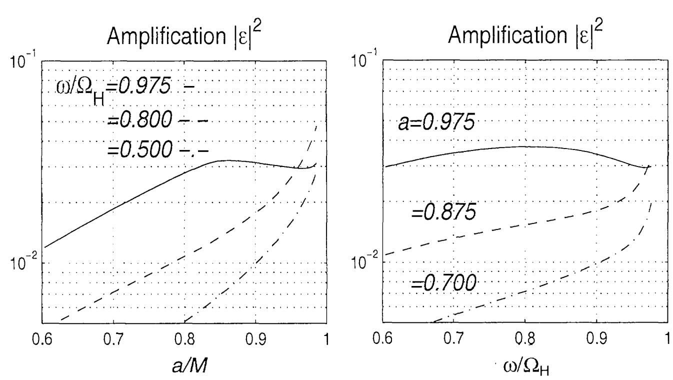


**Fig. 3.** The efficiency $|\epsilon|^2$ of superradiant amplification of a scalar field $\Phi$ of frequency $\omega$, estimated by the WKB method for $m = 1$ and shown as a function of $a/M$ (left) and $\omega/\Omega_H$ (right). The efficiency is a few percent for $a/M \geq 0.90$, which contains 50% of the rotational energy in the black hole, and $\omega/\Omega_H \geq 0.50$. This efficiency serves as a lower bound for that of the superradiant magnetosonic waves.

$$\Delta(\Delta\Phi')' + W\Phi = 0, W = [(r^2 + a^2)\omega - am]^2 - (m - a\omega)^2\Delta \qquad (1)$$

Here $\Phi$ is outgoing on the horizon when $0 < \omega < m\Omega_H$. A simultaneous transformation of the dependent and independent variables, $\Phi = Z/h$ and $\Delta d/dr = h^2/dx$ brings Eq. 1 into canonical form (*28*). The choice $\omega r'(x) = (e^{-x/\kappa} + 1)^{-1}$, where $x$ and $\kappa$ are dimensionless, gives $\omega r = \omega r_H + \kappa \ln(1 + e^{x/\kappa})$. Asymptotically, $\omega r'(x) \sim 1$ as $x \to \infty$, whereas near the horizon $\omega r'(x) \sim e^{x/\kappa}$ as $x \to -\infty$. Then $h$ is found to be $h^{-1} = \sqrt{r'/\Delta}$ and $2\kappa\sqrt{M^2 - a^2} = (a/\Omega_H)(m\Omega_H - \omega)$. This yields the transformed wave equation

$$Z'' + (1 - v)Z = 0 \qquad (2)$$

with normalized potential $v = 1 - Q$, where $Q = (W - h^3h'')/h^4$ such that $v(-\infty) = v(\infty) = 0$. The asymptotic radiation conditions are $Z \sim \epsilon e^{-i(t - x)}$ as $x \to -\infty$ and $Z \sim \epsilon e^{-i(t + x)} + be^{-i(t - x)}$ as $x \to \infty$. These conditions match those of an ordinary scattering viewed backward in time. As plotted in Fig. 3, WKB theory (*21*) predicts

$$|\epsilon|^2 \sim \exp(-2\int_{x_A}^{x_B} \sqrt{v - 1}dx)$$

where $v \geq 1$ on the interval $[x_A, x_B]$. The calculations show superradiance to be a few percent when $a/M \geq 0.90$ (and $\omega/\Omega_H \geq 0.50$). The mass-energy of the black hole may be parameterized as $M = M_i/\cos(\lambda/2)$, where $M_i$ is the irreducible mass and $\sin\lambda = a/M$ (*29*). Thus, 50% (90%) of the rotational energy $E_H^{rot} = M - M_i$ is within 10% (50%) of the maximum $a = M$. A positive-energy, narrow-band wave packet of azimuthal quantum number $m$ about $0 < \omega < m\Omega_H$ bounces in the cavity between the turning point of the barrier in the gravitational potential and the surface of the torus. Here $\omega$ is one of the standing-wave frequencies $\omega_l = lc\pi/L$, $l = 1,2,\cdots$ in the cavity with separation $L$ between the potential barrier and the torus. For $m = l = 1$, a lower bound on the cycle time $\tau = 2L/c$ follows from $\omega_1 = c\pi/L < \Omega_H \leq 1/2M$, namely $\tau > 4\pi M/c$. The growth per cycle is $\ln|b|^2 \sim |\epsilon|^2$, and it produces an expanding bubble in the cavity. The bubble either grows into dissipative equilibrium by Landau damping or radiative losses, or it ends in a burst.

Superradiance requires input, which may derive from radio emission $L_R$ coming off the torus. Such small-amplitude disturbances are expected to be broadband and to arise from turbulent shear flow in the torus resulting from the powerful torques acting on it. Here $L_R$ may be a tiny fraction of the turbulent dissipation $\sim L_H$, with some dependence on the partial pressure of the magnetic field in the torus. Let $f_{11}L_R$ denote the emission of waves into the cavity with angular dependence $m = 1$ and frequencies on the order of $\omega_1$. A single e-folding takes $N_0 \sim 1/|\epsilon|^2$ reflections, or a time $\tau_e \sim N_0 2L/c = 4\pi M/|\epsilon|^2 \sim 40(M/7M_\odot)(1\%/|\epsilon|^2)$ ms. Let $\mathscr{E}(t)$ denote the resonant energy in the cavity at time $t$. Then $\mathscr{E}(t) \sim tf_{11}L_R/Q$ $(t \leqslant \tau_e)$, where $Q$ is the "quality-factor" of the cavity, and $\mathscr{E}(t) \sim \mathscr{E}\tau_e\exp([t - \tau_e]/\tau_e)$ $(t \geqslant \tau_e)$. The time to equipartition with the energy $\mathscr{E}_m \sim B^2R^2 M/4$ in the magnetosphere is given by

$$T_{eq} = \tau_e \ln\left\{\left(\frac{eQ}{f_{11}}\frac{L_H}{L_R}\right)\left(\frac{\mathscr{E}_m}{\tau_e L_H}\right)\right\}$$

$$\sim 0.75\left(\frac{1\%}{|\epsilon|^2}\right)\left(\frac{M}{7M_\odot}\right) \text{s} \sim 0.15 \text{ to } 1.5 \text{ s} \qquad (3)$$

assuming an efficiency $|\epsilon|^2 = 0.5$ to 5% and a mass $M = 7M_\odot$. Here, $\mathscr{E}_m/\tau_e L_H \sim 4 \times 10^2|\epsilon|^2$ for $R \sim 8M$, whereby $L_H \sim 3 \times 10^{-3}B^2M^2$ when $a \sim M$. For $B = 10^{16}$ G, for example, $\mathscr{E}_m$ reaches 10% of the potential energy of the torus in the gravitational field of the black hole. Fiducial values are used for the unknown quantities, namely $L_R = 0.01L_H$, $Q = 100$, and $f_{11} = 10^{-3}$, where the latter is a rough estimate from expected infrared breaks in the spectral energy density of the turbulence at wave number $k^* \sim 6k_1 = 6/R$ and, correspondingly, $\omega^* \sim 6\omega_1$.

It has been suggested that the rotational energy from the hole is important in the fireball model of cosmological $\gamma$-ray bursts (*30*, *31*). For example, $4 \times 10^{53}$ erg can be derived at 10% efficiency from $E_H^{rot} \sim 2M_\odot$ in a $7M_\odot$ black hole, when it spins rapidly and is surrounded by the torus at $R \sim 8M$. This energy can be extracted in $T^* = 100$ s by $B \sim 10^{16}$ G, whence $L_H \sim 0.002M_\odot$/s. This requires a torus density of at least $10^9$ g/cm$^3$. If the torus has a mass of $1.35M_\odot$, then a prolonged black-hole/torus interaction is indeed possible because $R > R_c = 7.9M_\odot$. The fireball is believed to be powered by a Poynting flux-dominated-jet (*31*). If connected to the extended torus magnetosphere, bursting bubbles will modulate such a jet with internal shocks, consistent with intermittency at the source (*31*, *32*). Neglecting the time needed for the magnetosphere to regenerate, Eq. 3 implies a total number of subbursts (*31*) on the order of

$$\mathcal{N} \sim \frac{T^*}{T_{eq}} \sim 40 \text{ to } 400 \left(\frac{T^*}{60 \text{ s}}\right)$$

$$(|\epsilon|^2 = 0.5 \text{ to } 5\%) \qquad (4)$$

This intermittency, together with the ample reservoir $E_H^{rot} \geqslant m_{NS}$ available at 10% efficiency, and some expected diversity in angular momentum $J_H = aM$, provide the best evidence yet for the black-hole/torus model of cosmological $\gamma$-ray bursts.

The spiral-in phase of the coalescence of a NS/BH binary generates a rapidly increasing frequency chirp in gravitational radiation (up to $\sim 420$ Hz for breakup at $R \sim 8M$ around a $7M_\odot$ black hole) until a torus forms. In the present model, the $\gamma$-ray burst takes place in the black-hole/torus state, which is nearly quiescent in gravitational waves. When the torus begins to plunge into the hole, the $\gamma$-ray burst terminates and the gravitational radiation reappears in the form of quasi-normal mode ringing (*33*) of the horizon. Thus, our model predicts a $\gamma$-ray burst to be anticorrelated with its gravitational-wave emission. Its predecessor, the NS/BH binary, is not expected to have moved ultrarelativistically. Hence, beaming of its gravitational radiation should be negligible. For a given threshold of observable intensity of gravitational waves by the upcoming gravitational-wave detectors LIGO/VIRGO, the model predicts bursts of gravitational waves to outnumber the associated observable $\gamma$-ray bursts by a factor of about $2\pi/\theta^2 - 1$, where $\theta$ is the opening angle of a two-sided jet in the fireball model of $\gamma$-ray bursts.

### References and Notes


1. Y. Tanaka and W. H. G. Lewin, in *Black Hole Binaries*, W. H. G. Lewin, J. van Paradijs, E. P. J. van den Heuvel, Eds. (Cambridge Univ. Press, Cambridge, 1997), p. 126.
2. S. E. Thorsett and D. Chakrabarty, *Astrophys. J.* **512**, 288 (1999).
3. B. Paczynski, *Acta Astron.* **41**, 257 (1991).
4. E. Costa *et al.*, *Nature* **387**, 783 (1997); M. R. Metzger *et al.*, *ibid.*, p. 878.
5. C. D. Bailyn, R. K. Jain, P. Coppi, J. A. Orosz, *Astrophys. J.* **499**, 367 (1998).
6. J. M. Lattimer and D. N. Schramm, *ibid.* **210**, 549 (1976); *Astrophys. J. Lett.* **192**, L145 (1974).
7. A Schwarzschild black hole of mass $M$ is described by the line-element

$$ds^2 = -\left(1 - \frac{2M}{r}\right)dt^2 + \frac{dr^2}{1 - \frac{2M}{r}}dr^2 + r^2(d\theta^2 + \sin^2\theta\, d\phi^2).$$

Asymptotically for large $r$, it takes the appearance of an ordinary Newtonian particle whose potential is $M/r$. Nearby, it is characterized by an event horizon at $r = M$, where the redshift $z = (1/\alpha) - 1$, where

$$\alpha = \sqrt{1 - \frac{2M}{r}}$$

approaches infinity: The evolution of an infalling observer appears to "freeze out" relative to observers at large distances [see, for example, (*13*)].
8. A rotating black hole of mass $M$ and specific angular momentum $a$ is described by the axisymmetric, stationary Kerr metric, for example, in a line-element of the form (*13*) $ds^2 = -\alpha^2dt^2 + g_{jk}(dx^j + \beta^j)(dx^k + \beta^k dt)$. The shift vector $\beta$ describes frame-dragging in its exterior space-time, which introduces certain novel features. Of interest here is the interaction of $\beta$ with a surrounding magnetic field, $B$, which is described by an additional Lie derivative $J_\beta = \mathscr{L}_\beta B$ in Faraday's law [Eq. 3.52 in (*13*)]. This may be viewed as a current of virtual magnetic charges. In a force-free magnetosphere, the magnetic field–lines become equipotentials, so that $J_\beta$ produces a potential difference only across the field lines. Thus, field lines that penetrate the black hole can have their potentials labeled by a virtual polarization on its horizon, which is essentially the viewpoint in (*19*) [see also Eqs. 3.103 to 3.106 in (*13*)].
9. L. G. Fishbone, *Astrophys. J.* **175**, L155 (1972).
10. H. A. Bethe and G. E. Brown, preprint available at http://xxx.lanl.gov/abs/astro-ph/9805355.
11. J. M. Bardeen, *Nature* **226**, 64 (1970).
12. D. Lai, preprint available at http://xxx.lanl.gov/abs/astro-ph/9806378.
13. K. S. Thorne, R. H. Price, D. A. MacDonald, *The Membrane Paradigm* (Yale Univ. Press, New Haven, CT, 1986).

14. P. Goldreich and W. H. Julian, *Astrophys. J.* **157**, 869 (1969).
15. R. M. Wald, *Phys. Rev. D.* **10**, 1680 (1974).
16. See Eq. 3.108 in (*13*).
17. S. L. Shapiro and S. A. Teukolsky, *Black Holes, White Dwarfs, and Neutron Stars* (Wiley, New York, 1983).
18. R. L. Znajek, *Mon. Not. R. Astron. Soc.* **179**, 457 (1977).
19. R. D. Blandford and R. L. Znajek, *ibid.*, p. 433.
20. J. Arons and J. J. Barnard *Astrophys. J.* **302**, 120 (1986); *ibid.*, p. 138.
21. T. Uchida, *Mon. Not. R. Astron. Soc.* **291**, 125 (1997).
22. C. Thompson, *ibid.* **270**, 480 (1994).
23. V. Canuto and C. Chiuderi, *Phys. Rev. D.* **1**, 2219 (1970).
24. W. H. Press and S. A. Teukolsky, *Nature* **238**, 211 (1972).
25. J. M. Bardeen, W. H. Press, S. A. Teukolsky, *Astrophys. J.* **178**, 347 (1972).
26. Ya. B. Zel'dovich, *Zh. Eks. Teor. Fiz.* **14**, 270 (1971) [transl. *JETP Lett.* **14**, 180 (1971)].
27. S. A. Teukolsky and W. H. Press, *Astrophys. J.* **193**, 443 (1974).
28. S. A. Teukolsky, *ibid.* **185**, 635 (1973).
29. $\sin\lambda = a/M$ is a convenient parameterization for Kerr black hole parameters, including $\Omega_H = \tan(\lambda/2)/2M$ and $J_H = M^2 \sin\lambda$, whose adiabatic evolution is given by $\dot{\Omega}_H = \dot{\lambda}/4M$ and $\dot{J}_H = M^2\dot{\lambda}$.
30. M. J. Rees, in *18th Texas Symposium on Relativistic Astrophysics and Cosmology*, A. V. Olinto, J. A. Frieman, D. N. Schramm, Eds. (World Scientific, Singapore, 1998), pp. 34–47.
31. T. Piran, preprint available at http://xxx.lanl.gov/abs/astro-ph/9810256.
32. T. Piran and R. Sari, in (*30*), pp. 494–496.
33. W. H. Press *Astrophys. J.* **170**, L105 (1971).



34. I gratefully acknowledge stimulating discussions with A. Toomre and J. M. Bardeen, and thank R. D. Blandford for drawing attention to reference 21. This research was supported by NASA grant NAG5-7012.

30 September 1998; accepted 1 March 1999


# Geochemical Consequences of Increased Atmospheric Carbon Dioxide on Coral Reefs


**Joan A. Kleypas,[1]* Robert W. Buddemeier,[2] David Archer,[3] Jean-Pierre Gattuso,[4] Chris Langdon,[5] Bradley N. Opdyke[6]**



A coral reef represents the net accumulation of calcium carbonate ($CaCO_3$) produced by corals and other calcifying organisms. If calcification declines, then reef-building capacity also declines. Coral reef calcification depends on the saturation state of the carbonate mineral aragonite of surface waters. By the middle of the next century, an increased concentration of carbon dioxide will decrease the aragonite saturation state in the tropics by 30 percent and biogenic aragonite precipitation by 14 to 30 percent. Coral reefs are particularly threatened, because reef-building organisms secrete metastable forms of $CaCO_3$, but the biogeochemical consequences on other calcifying marine ecosystems may be equally severe.


Atmospheric $CO_2$ is expected to reach double preindustrial levels by the year 2065 (*1*). $CO_2$ research in the marine environment has focused on the ocean's role in sequestering atmospheric $CO_2$ (*2, 3*), but the potential effects of the resulting ocean chemistry changes on marine biota are poorly known.

Dissolved inorganic carbon occurs in three basic forms: $CO_2$* ($CO_{2(aq)} + H_2CO_3$), $HCO_3^-$, and $CO_3^{2-}$. Under normal seawater conditions (pH 8.0 to 8.2), [$HCO_3^-$] is roughly 6 to 10 times [$CO_3^{2-}$]. When $CO_2$ dissolves in seawater, less than 1% remains as $CO_2$*; most dissociates into $HCO_3^-$ and $CO_3^{2-}$, and the acid formed by dissolution of $CO_2$ in seawater lowers the pH so that some $CO_3^{2-}$ combines with $H^+$ to form $HCO_3^-$. Thus, addition of fossil fuel $CO_2$ decreases [$CO_3^{2-}$].

The seawater-mediated interaction of $CO_2$ and calcium carbonate ($CO_2 + H_2O + CaCO_3 \leftrightarrow 2HCO_3^- + Ca^{2+}$) illustrates how addition of $CO_2$ enhances $CaCO_3$ dissolution and removal of $CO_2$ enhances its precipitation. Calcium carbonate saturation state ($\Omega$) is

$$\Omega = \frac{[Ca^{2+}][CO_3^{2-}]}{K'_{sp}}$$

where $K'_{sp}$ is the stoichiometric solubility product for a particular mineral phase of $CaCO_3$ [calcite (calc), aragonite (arag), or high-magnesian calcite (hmc)]. $\Omega$ is largely determined by [$CO_3^{2-}$] because [$Ca^{2+}$] is near conservative in seawater. Tropical surface waters are supersaturated ($\Omega > 1.0$) with respect to all mineral phases, but the degree of saturation varies: $\Omega$-calc is 5 to 6, $\Omega$-arag is 3 to 4, and $\Omega$-hmc is 2 to 3. Under the worst case global change scenarios of the Intergovermental Panel on Climate Change (IPCC), the surface ocean will remain almost entirely supersaturated with respect to $CaCO_3$, but the decreased saturation state could result in reduced calcification rates, a shift toward calcite secretors, or a competitive advantage for noncalcifying reef organisms (*4*).

Shifts in carbonate mineralogy over geologic time appear to coincide with inferred atmospheric $CO_2$ concentrations (*5*), and the latitudinal trends of Phanerozoic carbonate accretion rates correlate well with saturation state (*6*). Current reef distribution also correlates with saturation state (*7*), and large-scale biogeochemical studies have found a positive relationship between saturation state and calcification (*8*). Fragile coral skeletons have been reported from high-latitude, low $\Omega$-arag reefs and coral communities (*9*), and reefs in well-mixed, highly supersaturated waters such as the Red Sea tend to have abundant internal carbonate cements (*10*), whereas those in low saturation waters such as the eastern Pacific have none (*11*). Modern aragonitic ooids and "whitings" also form only where $\Omega$-arag is high (for example, Bahama Banks, Persian Gulf).

Experimental studies of calcification versus saturation state in marine organisms or communities are rare. In a recent review (*12*), six such studies on corals and marine algae (the major reef-building taxa) were identified, and, despite methodological differences, all showed a significant positive correlation between saturation state and calcification. Recent experiments in the Biosphere 2 coral reef mesocosm show a strong dependence of community calcification on saturation state (*13*).

We used two methods to predict changes in surface saturation state. The first assumed constant alkalinity through the middle of the next century and that ocean surface response to increased $P_{CO_2}$atm is strictly thermodynamic ($P_{CO_2}$surf is near equilibrium with $P_{CO_2}$atm) (*14*). This is valid in the tropics except for upwelling regions (*3*). The second method employed the HAMOCC (Hamburg Ocean Carbon Cycle) global model (*15*), which simulates response of the entire carbon system to increased $P_{CO_2}$atm and can thus be used to project further into the future. In this model biogeochemical tracers are advected with a frozen present-day climatological flow field, neglecting the possibility of future changes in ocean circulation (*16*).

Both methods indicate a significant drop in $\Omega$-arag as $P_{CO_2}$atm increases (Fig. 1, A and B). The HAMOCC model $\Omega$-arag values are consistently lower than the thermodynamic calculations because of slightly different global change scenarios and differences between modeled and measured alkalinity. Otherwise the two methods produce similar trends (Fig. 1C). Average $\Omega$-arag in the tropics 100 years ago


[1]National Center for Atmospheric Research, Boulder, CO 80307, USA. [2]Kansas Geological Survey, University of Kansas, Lawrence, KS 66047, USA. [3]Department of Geophysical Sciences, University of Chicago, Chicago, IL 60637, USA. [4]Observatoire Océanologique, ESA 7076 CNRS-UPMC, B.P. 28, F-06234 Villefranche-sur-mer Cedex, France. [5]Lamont-Doherty Earth Observatory, Palisades, NY 10964, USA. [6]Department of Geology, Australian National University, Canberra, ACT 0200, Australia.

*To whom correspondence should be addressed. E-mail: kleypas@ncar.ucar.edu